Front. Chem. Sci. Eng. 2018, 12(2): 283–295
https://doi.org/10.1007/s11705-017-1687-2

RESEARCH ARTICLE

Head-to-tail cyclization of a heptapeptide eliminates its cytotoxicity and significantly increases its inhibition effect on amyloid β-protein fibrillation and cytotoxicity

Shuai Ma[1], Huan Zhang[1], Xiaoyan Dong (✉)[1], Linling Yu[1], Jie Zheng[2], Yan Sun[1]

1 Department of Biochemical Engineering and Key Laboratory of Systems Bioengineering of the Ministry of Education, School of Chemical Engineering and Technology, Tianjin University, Tianjin 300350, China
2 Department of Chemical and Biomolecular Engineering, The University of Akron, Akron, OH 44325, USA

Abstract Amyloid-β (Aβ) protein aggregation is the main hallmark of Alzheimer's disease (AD). Inhibition of Aβ fibrillation is thus a promising therapeutic approach to the prevention and treatment of AD. Recently, we designed a heptapeptide inhibitor, LVFFARK (LK7). LK7 shows a promising inhibitory capability on Aβ fibrillation, but is prone to self-assembling and displays high cytotoxicity, which would hinder its practical application. Herein, we modified LK7 by a head-to-tail cyclization and obtained a cyclic LK7 (cLK7). cLK7 exhibits a different self-assembly behavior from LK7, and has higher stability against proteolysis than LK7 and little cytotoxicity to SH-SY5Y cells. Thermodynamic analysis revealed that both LK7 and cLK7 could bind to $A\beta_{40}$ by electrostatic interactions, hydrogen bonding and hydrophobic interactions, but the binding affinity of cLK7 for $A\beta_{40}$ (K_D = 4.96 μmol/L) is six times higher than that of LK7 (K_D = 32.2 μmol/L). The strong binding enables cLK7 to stabilize the secondary structure of $A\beta_{40}$ and potently inhibit its nucleation, fibrillation and cytotoxicity at extensive concentration range, whereas LK7 could only moderately inhibit $A\beta_{40}$ fibrillation and cytotoxicity at low concentrations. The findings indicate that the peptide cyclization is a promising approach to enhance the performance of peptide-based amyloid inhibitors.

Keywords Alzheimer's disease, amyloid β-protein, cyclic peptide, inhibition, protein aggregation

1 Introduction

Alzheimer's disease (AD) is the most prevalent neurodegenerative disease and a major case of dementia [1]. Although the precise mechanism of AD pathogenesis has not been completely understood, amyloid β-protein (Aβ) aggregates into extracellular senile plaques has been recognized as the main hallmark of AD [2]. Aβ aggregation is generally described by a nucleation-growth model, in which Aβ successively aggregates into oligomers, protofibrils, and finally mature fibrils [3]. Extensive evidence has demonstrated that soluble Aβ oligomers [4] and protofibrils [5] are the most toxic species to neuron cells. Therefore, inhibition of Aβ aggregation to oligomers and protofibrils at the early stage has been considered as a promising strategy for preventing or delaying the progression of AD.

Many efforts have been made to develop potent amyloid inhibitors, including small molecules, chaperone proteins, peptides, peptide mimics, nanoparticles, and antibodies [6,7]. Of those, the peptide-based inhibitors offer several advantages over other inhibitors: high target affinity, ease of synthesis and modification, and favorable biocompatibility [8]. Because some Aβ fragments could interact with homologous sequence of full-length Aβ molecules via hydrophobic interactions and hydrogen bonding, Aβ fragments have been used as starting materials, such as $A\beta_{16\text{-}20}$ (KLVFF) [9,10], $A\beta_{17\text{-}21}$ (LVFFA) [11], $A\beta_{32\text{-}37}$ (IGLMVG) [12] and $A\beta_{37\text{-}42}$ (GGVVIA) [13]. Among them, $A\beta_{16\text{-}20}$ (KLVFF) or $A\beta_{17\text{-}21}$ (LVFFA) is the hydrophobic core of the full-length Aβ and plays an important role in Aβ fibrillation [14]. However, the inhibitory effect of this fragment is marginal, so researchers have tried to modify it to find more effective inhibitors [15,16]. Previously, our group designed a heptapeptide

Received July 8, 2017; accepted September 19, 2017

E-mail: d_xy@tju.edu.cn

LVFFARK (LK7, Scheme 1(a)), based on the analysis of molecular interaction with Aβ [17]. LK7 did exhibit a superior inhibitory effect on Aβ aggregation over LVFFA, but it was prone to self-assembling, resulting in the formation of toxic species. Hence, there is a need to further modify LK7 to improve its performance in inhibiting amyloid aggregation and cytotoxicity.

Recently, several cyclic peptides have been designed to inhibit Aβ aggregation [18–22]. It has been proved that, the different topological features of a linear peptide and its corresponding cyclic peptide can significantly affect their physiochemical and biological properties [23]. Moreover, it has been reported that cyclization of a linear peptide inhibitor would strengthen its binding affinity for amyloid fibrils and enhance its efficacy to eliminate cytotoxic Aβ species by transition of toxic low-molecular-weight Aβ oligomers into less toxic Aβ-cyclic-peptide co-precipitates of high molecular weights [24]. Inspired by these findings, we have thus developed a cyclic LK7 (cLK7, Scheme 1(b)) by a head-to-tail cyclization for an enhanced capability against Aβ aggregation and cytotoxicity. Besides, it is expected that the head-to-tail cyclization could enhance the stability of the peptide against proteolysis [25] and its membrane permeability [26]. Therefore, the physiochemical and biological properties of LK7 and cLK7 were determined, including their aggregation behaviors, resistance against enzymatic hydrolysis and cytotoxicity. Then, extensive biophysical and biological assays were conducted to explore the influence of LK7 and cLK7 on Aβ_{40} fibrillation and cytotoxicity at different concentrations, and analyze whether the cyclization could enhance the inhibitory effect.

2 Materials and methods

2.1 Materials

Dimethyl sulfoxide (DMSO), 1,1,1,3,3,3-hexafluoro-2-propanol (HFIP), and thioflavin T (ThT) were purchased from Sigma-Aldrich (St. Louis, MO, USA). Aβ_{40} was obtained from GL Biochem (Shanghai, China). Linear LK7 (Ac-LVFFARK-NH_2) ($>95\%$ purity) and cyclic peptide cLK7 ($>95\%$ purity) were provided by ZYBio (Shanghai, China). α-Chymotrypsin from bovine pancreas (EC 3.4.21.1, >1000 USP U/mg) was received from Sangon Biotech (Shanghai, China). 3-(4,5-Dimethylthiazol-2-yl)-2,5-diphenyltetrazolium bromide (MTT) was purchased from Dingguo Biotech (Beijing, China). The cell line SH-SY5Y was provided by the Cell Bank of Chinese Academy of Science (Beijing, China). Fetal bovine serum (FBS) and Dulbecco's Modified Eagle Medium/Ham's F-12 (DMEM/F12) were purchased from Gibco Invitrogen (Grand Island, NY, USA). All other chemicals were the highest purity available from local sources.

2.2 Aβ_{40} preparation

Aβ_{40} solution was prepared as described by Wang et al. [27] Briefly, a sample of Aβ_{40} powder was dissolved in HFIP to 1 mg/mL and kept steady for 2 h. The solution was then sonicated for 3 min in ice bath, and centrifuged for 30 min at 15000 g and 4 °C to remove pre-existing Aβ_{40} aggregates. About 75% of the supernatant was collected and the solvent was removed by vacuum freeze-drying overnight. Before use, Aβ_{40} was dissolved in 20 mmol/L NaOH, centrifuged for 20 min at 16000 g and 4 °C to remove aggregates, and then diluted with phosphate buffered saline (PBS) solution (100 mmol/L phosphate buffer plus 10 mmol/L NaCl, pH 7.4) to a desired concentration.

2.3 Inhibitor solution preparation

The heptapeptide, LK7 or cLK7, was first dissolved in DMSO and diluted with the PBS to form a stock peptide solution (1 mmol/L) containing 10% DMSO. The stock

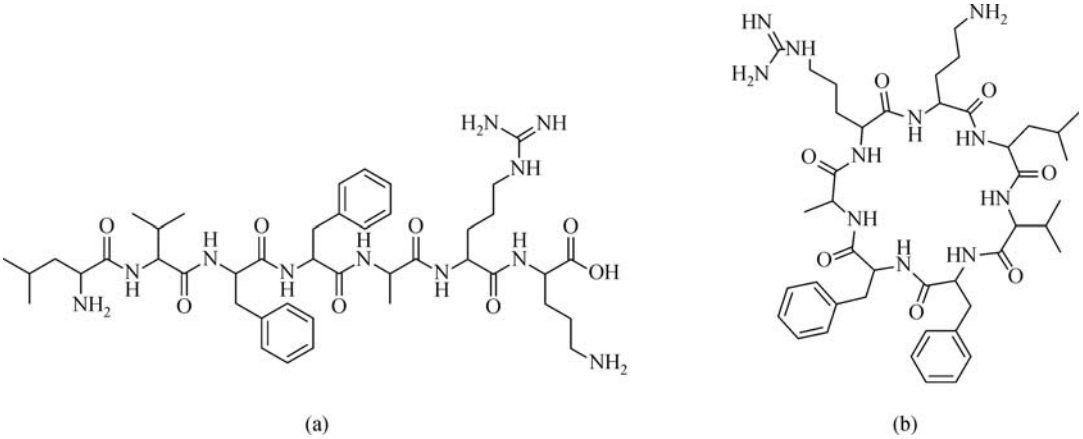

Scheme 1 Chemical structures of (a) LK7 and (b) cLK7

solution was diluted with the PBS to different concentrations for the following uses. Thus, the samples in the inhibition experiments were composed of 25 μmol/L Aβ_{40} and different peptide inhibitor concentrations in the PBS with 2% DMSO.

2.4 α-Chymotrypsin degradation assay

α-Chymotrypsin was used to explore the ability of heptapeptide to resist enzymatic hydrolysis [28], following the procedure reported previously [29,30]. α-Chymotrypsin (50 μmol/L) was dissolved in a buffer comprised of 50 mmol/L Trizma base, 100 mmol/L sodium chloride, 10 mmol/L calcium chloride di-hydrate filtered in deionized water (pH 8.08). The peptide solutions were freshly prepared at 200 μmol/L. For each assay, samples were incubated at 37 °C for different time intervals (0 to 20 h). The sample for each assay consisted of a mixture of 350 μL peptide solution and 50 μL of enzyme solution. Each sample was quenched by addition of 3 μL of 25% (v/v) acetic acid in deionized water. Reversed-phase high-performance liquid chromatography (RP-HPLC) was used to monitor the progress of each reaction, with a C_{18} reversed-phase column (Waters, Milford, MA, USA) connected to an Agilent 1100 Series HPLC system (Agilent Technologies, Santa Clara, CA) operated at 0.8 mL/min using a linear gradient of 10%–70% acetonitrile with 0.1% trifluoroacetic acid. The amount of intact peptide remaining was determined by integration of the peak detected at 210 nm. Each trial was performed for three times, and the average value is reported with a standard deviation.

2.5 ThT fluorescent assay

Aβ_{40} aggregation in the presence and absence of inhibitors was monitored by ThT fluorescent assay. Aliquots of incubation solutions at different time intervals were taken and diluted 20 times into ThT solutions (25 μmol/L ThT in 25 mmol/L phosphate buffer, pH 6.0). ThT fluorescence was measured by a fluorescence spectrophotometer (LS-55, PerkinElmer, USA) with a slit width of 5 nm at 25 °C, excitation and emission at 440 and 480 nm, respectively.

For kinetic analysis, samples were prepared by mixing 25 μmol/L Aβ_{40} monomers, 25 μmol/L ThT and different concentrations of inhibitors in PBS buffer (100 mmol/L sodium phosphate, 10 mmol/L NaCl, pH 7.4). The samples (200 μL) were added in a black 96-well flat-bottom plate, and the fluorescence of amyloid-bound ThT was measured for 72 h using a fluorescence plate reader (Infinite M200 Pro, Tecan, Switzerland) at 15 min reading intervals and 5 s shaking before each reading. The wells were prepared in hexaplicate, and three representative data were selected for calculating the average fluorescence signals, which were subtracted by the baseline fluorescence of the control samples without Aβ_{40} [31]. Each experiment was performed in triplicate, and the most representative curve was reported. The kinetic growth curves of aggregation were normalized using a sigmoidal fit equation [32]:

$$y = y_0 + \frac{y_{\max} - y_0}{1 + \exp[-(t - t_{1/2})]k}, \quad (1)$$

where y is the fluorescence intensity at time t, y_0 and $y_{\max}$ are the minimum fluorescence intensities (pre-transition) and maximum fluorescence intensities (post-transition), respectively, $t_{1/2}$ is the time when the fluorescence intensity reaches half the maximum intensity, and k is the apparent first-order aggregation constant. The lag phase time (T_{lag}) can be calculated from $T_{\text{lag}} = t_{1/2} - 2/k$, and the completion time is $t_{1/2} + 2/k$. Thus it can be deduced that the total transition time T_{trans} is $4/k$ [33].

2.6 Transmission electron microscopy (TEM)

The morphologies of Aβ_{40} with or without inhibitors, and LK7 and cLK7 aggregates were observed with a JEM-100CXII TEM system (JEOL Inc., Tokyo, Japan) on an accelerating voltage of 100 kV. The samples were diluted to appropriate concentrations, dropped onto carbon-coated copper grids (400-mesh), and air-dried for 5 min. Then, the samples were negatively stained using 2% (w/v) phosphotungstic acid for 5 min, and the excess solution was removed by filter paper. Each TEM observation was conducted at least at four different locations, and representative images are reported.

2.7 Circular dichroism (CD) spectroscopy

The CD spectra of the peptides alone and Aβ_{40} (25 μmol/L) in the absence and presence of the peptides at 25, 50, 100, 200 μmol/L were recorded using a J-810 spectrometer (Jasco, Japan) at 37 °C. A quartz cell with 1 mm path length was used for far-ultraviolet (UV, 200–260 nm) measurements with 1 nm bandwidth, and the scanning speed was 50 nm/min with a continuous scanning mode. The spectrum for each peptide alone was subtracted from the spectrum of Aβ_{40}/peptide solution, to leave normalized CD spectra accounting for the effect of the peptide upon Aβ_{40}. Simultaneously, the influence of DMSO in the solution on the CD signal was also eliminated, as done in literature [22]. Each CD spectrum was the average of three consecutive scans for each sample. To obtain quantitative information on the structural transition, the secondary structure contents of the peptide samples were analyzed using the BeStSel method provided by the BeStSel website [34].

2.8 Isothermal titration calorimetry (ITC)

ITC experiments were performed using a VP isothermal titration calorimeter (MicroCal, Northampton, MA) in PBS (100 mmol/L sodium phosphate, 10 mmol/L NaCl, pH 7.4)

at 37 °C. A peptide solution of 275 μL was loaded in the injection syringe, and after an initial delay of 800 s, a 10 μL aliquot was continuously injected over 20 s for 25 times via a 307 r/min rotating stirrer-syringe into the sample cell. To ensure the consistency of the background, Aβ_{40} for this experiment was dissolved with DMSO and then diluted with PBS buffer to different concentrations, and the final solution contained 4% DMSO. The peptide concentration in the syringe was 400 μmol/L. Blank titrations, which were carried out by injecting peptides into buffer, were subtracted from each data set, as done in literature [35]. All sample solutions were degassed at 37 °C before the measurements, and the final molar ratios were 1 to 10 for Aβ_{40} to LK7 and 1 to 16 for Aβ_{40} to cLK7, respectively. These molar ratios ensured to obtain typical and reliable titration curves. The association constant K_A, enthalpy change ΔH were obtained from fitting the data using the single-site binding model in Microcal Origin 7.0 software. The dissociation constant K_D, the free energy change ΔG, and the entropy changes ΔS were obtained from the basic thermodynamic relationships:

$$K_D = K_A^{-1}, \tag{2}$$

$$\Delta G = -RT\ln K_A, \tag{3}$$

$$\Delta G = \Delta H - T\Delta S. \tag{4}$$

Herein, ΔG is calculated from K_D at T = 310.15 K (37 °C). The Wiseman's C-parameter was used to evaluate the binding simulation curves, which was defined as [36]:

$$C = n[M]/K_D, \tag{5}$$

where n is the number of binding sites per macromolecule M, and [M] is the total macromolecule concentration. A C value in the range of 1 to 1000 means accurate estimation of a K_D value [36,37]. Three replicates were performed for each experiment, and the average data were reported with standard deviations.

2.9 Cytotoxicity assay

Cell viability was determined by the MTT method [38], with SH-SY5Y cells widely used as *in vitro* cellular models for AD. SH-SY5Y cells were cultured in DMEM/F-12 medium, supplemented with 10% fetal bovine serum (FBS), 1% L-glutamine and 1% penicillin or streptomycin. The cultivation was maintained at 37 °C in an atmosphere of 5% CO_2. For cell viability assays, cells were plated in a 96-well plate at a density of about 5000 cells per-well with 80 μL fresh medium. After incubation for 24 h, the aged Aβ_{40} aggregates with different concentrations of inhibitors (20 μL each well) were added into the plates, and the cells were incubated for another 24 h. Then, 10 μL of MTT solution (5.5 mg/mL) was added to each well, and the plates were incubated for another 4 h. Thereafter, the culture medium was removed by centrifugation, and the precipitated cells were lysed using DMSO. After the purple crystal were dissolved completely, the cell viability was calculated from the absorbance signals measured by a plate reader (Infinite M200 PRO, Tecan, Switzerland) at 570 nm. The wells containing medium only were taken as the background and were subtracted from each reading. The cell viability data were normalized as a percentage of the control group without Aβ_{40} and an inhibitor. Six replicates were conducted and the averaged data with standard deviations are reported. Analysis of variance was carried out for statistical comparisons using t-test, and $p < 0.05$ or less was considered to be statistically significant.

3 Results and discussion

3.1 Characterization of LK7 and cLK7

As observed by TEM, both LK7 and cLK7 showed obvious self-assembly propensity, but the morphologies were significantly different. LK7 assembled into dense and long amyloid-like fibrils (Fig. 1(a)), but cLK7 aggregated into more distributed and spherical particles (Fig. 1(b)). The morphology of cLK7 aggregates was similar to the cyclic peptide aggregates reported in literature [23], though the cLK7 aggregates were much bigger (40–60 nm). Protease stability of the two peptides is presented in Fig. 1(c). It is seen that LK7 degraded rapidly, only about 1 h for half degradation. By contrast, cLK7 showed a significant α-chymotrypsin-resistant feature, with only about 8% degradation at 1 h, and the time for half degradation was over 7 h. The prolonged protease stability would increase the bioavailability of cLK7. The cytotoxicity of LK7 and cLK7 aggregates were then compared. As shown in Fig. 1(d), LK7 showed obvious cytotoxicity on SH-SY5Y cells, and the cell viability was only 63% for SH-SY5Y cells at 200 μmol/L. However, cLK7 presented less toxicity on the cells in the tested concentration range, and 93% cell viability was maintained at 200 μmol/L. The characterization displayed the superiority of cLK7 over LK7 in protease- resistance and cytotoxicity.

To provide more details about their aggregation behaviors, the conformational transitions of LK7 and cLK7 during their incubations were monitored by CD spectroscopy (Figs. S1(a) and S1(b)). The CD spectra of both LK7 and cLK7 displayed a distinct minimum of ellipticity around 200–202 nm, indicating that the peptides exist mostly in a random-coil state. In addition, a broad maximum ellipticity at 215–217 nm was observed on each spectrum, similar to the CD signature of the β-turn peptide containing aromatic residues, most likely originated from the intermolecular π-π interactions [39,40]. Furthermore, the estimated content quantitatively analyzed by the BeStSel method showed that antiparallel β-sheet, turn and other unordered structures were the three main

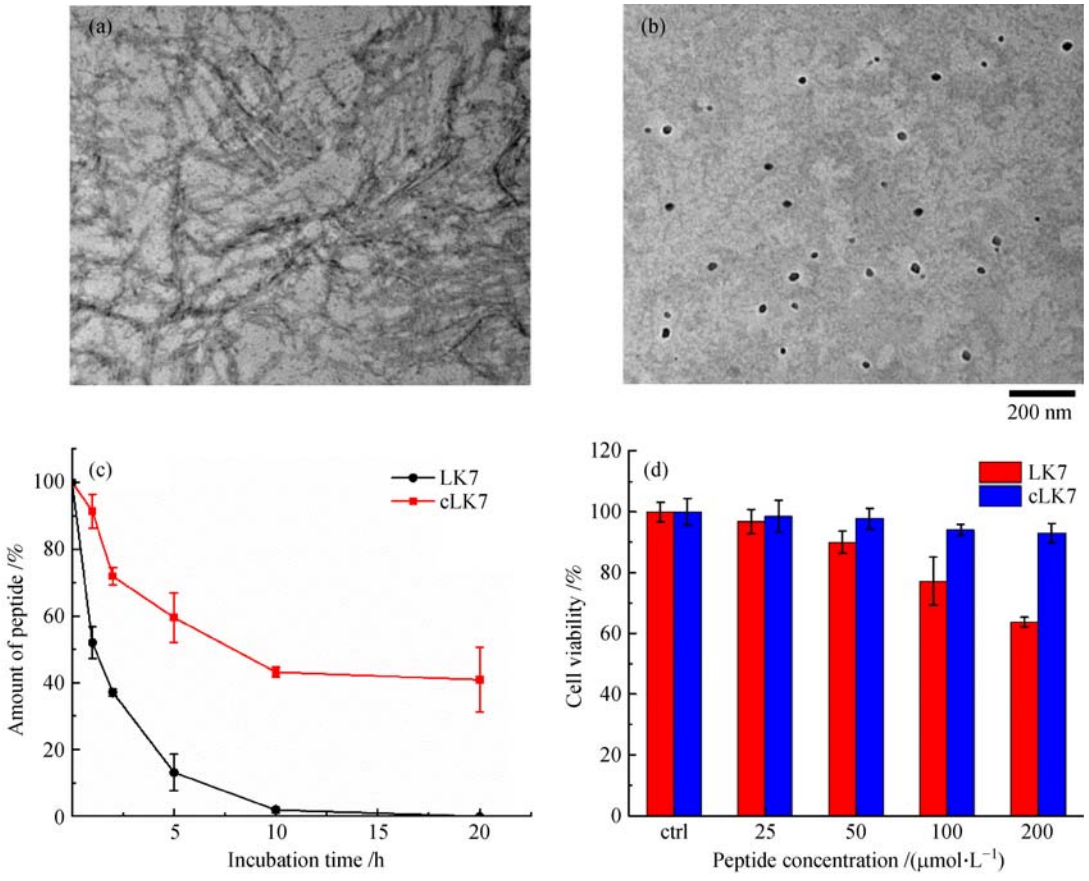

Fig. 1 Characterization of LK7 and cLK7. TEM images of (a) LK7 and (b) cLK7 (200 μmol/L for both) after incubation at 37 °C for 72 h. The scale bar of 200 nm is for the two images. (c) The time course of intact peptides by incubating with α-chymotrypsin. Error bars represent the standard deviation of the measurement (n = 3). (d) Cytotoxicity induced by LK7 and cLK7 aggregates detected using SH-SY5Y cells. In the MTT assay, the cell viability treated with PBS buffer alone was set to 100%

secondary structures (Table S1). These results indicate that the primary driving force for the self-assembly of both the linear and cyclic peptides were hydrophobic and π-π stacking interactions between phenylalanine residues [23] as well as hydrogen bonding. However, LK7 and cLK7 exhibited obvious differences in the contents of turn and unordered structures: The turn in LK7 was higher than in cLK7, but the unordered structures (others) in LK7 were lower than in cLK7. These differences would have contributed to their completely different aggregation behaviors.

3.2 Effects of LK7 and cLK7 on Aβ_{40} fibrillation

ThT dye can specifically bind to fibrillar aggregates with β-sheet structures, and the fluorescent signal is proportional to the amount of β-sheet structure [41], so we used ThT fluorescence assays to monitor Aβ_{40} fibrillation upon incubating with LK7 and cLK7. LK7 and cLK7 at different concentrations produced almost negligible ThT signals (Figs. S2(a) and S2(b)), so the interference of the peptides on detecting the ThT fluorescence of Aβ fibrillation was negligible. LK7 inhibited aggregation of Aβ_{40} in a dose-dependent manner at low concentration ($\leqslant$100 μmol/L), and a co-incubation of Aβ_{40} and LK7 in a molar ratio of 1:4 resulted in a 57% reduction in the fluorescent signal (Fig. S3). However, increase of LK7 concentration to 200 μmol/L (Aβ_{40} and LK7 in a molar ratio of 1:8) weakened the inhibitory effect, which is probably due to the fact that the self-assembly of LK7 reduced the available amount of LK7 for Aβ (Fig. 1(a)). By contrast, cLK7 effectively inhibited aggregation of Aβ_{40} in the tested concentration range of 25 to 200 μmol/L (Fig. S3). The fluorescent signal significantly decreased from 74% to 19% when the molar ratio of Aβ/cLK7 increased from 1:1 to 1:8. Additionally, by comparing the two peptides at the same concentrations, it is seen that the inhibitory effect of cLK7 was always better than LK7, indicating the superiority of cLK7 over LK7.

Besides the final fluorescent signal of fibrils, aggregation kinetics were performed by ThT fluorescence assays to investigate the effects of LK7 and cLK7 in different concentrations on Aβ_{40} fibrillation (Figs. 2(a) and 2(b)). Amyloid fibrillogenesis is generally thought to be a

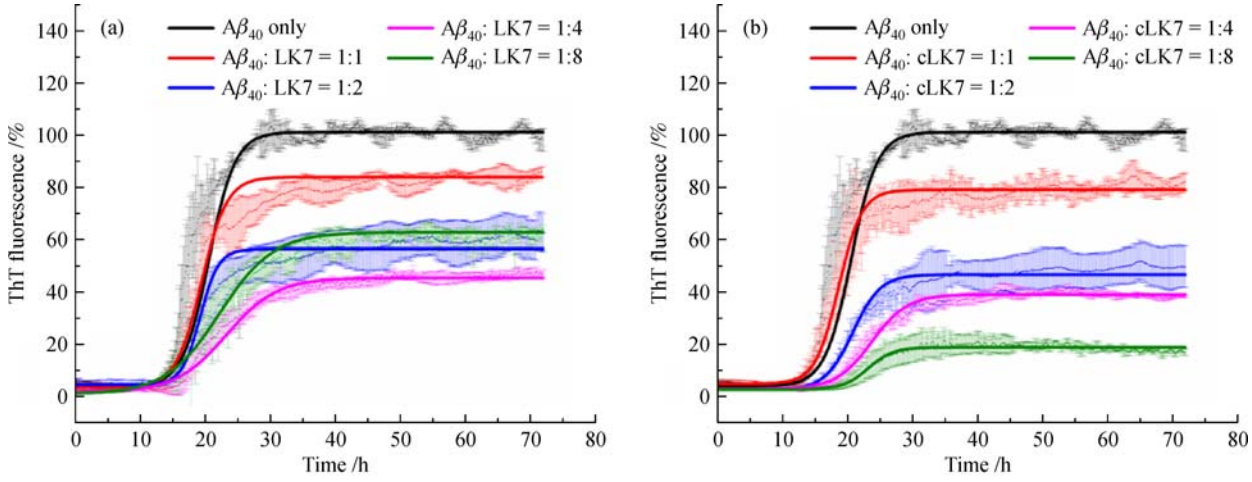

Fig. 2 Aggregation kinetics of Aβ_{40} incubated without and with different concentrations of (a) LK7, and (b) cLK7. Aβ_{40} concentration was 25 μmol/L

nucleation-dependent polymerization, typically displaying sigmoidal growth kinetics [42]. The lag time depicts the time required for the formation of critical nucleus [43], and the transition time represents the time of the nuclei growth into amyloid fibrils and reflects the elongation rate of the fibrils [33,44]. Lag times and transition times, calculated from Eq. (1), are listed in Table 1. For the case of Aβ_{40} alone, the lag time was 14.5 h and the transition time was 8.3 h (Table 1). When Aβ_{40} was co-incubated with LK7, there were no significant changes in the lag time at low concentrations ($\leqslant$100 μmol/L) (Fig. 2(a), Table 1). However, addition of 200 μmol/L LK7 shortened the lag time to 12.1 h, implying that LK7 in high concentration promoted the nucleation of Aβ_{40}. It is considered due to the self-assembly of LK7 (Fig. 1(a)), which facilitated clustering of Aβ_{40} monomers. In other words, the LK7 aggregates might act as catalytic sites for Aβ aggregation. Namely, Aβ monomers could bind to the LK7 aggregates, resulting in the higher local concentration of Aβ_{40} monomers, which might facilitate Aβ_{40} nucleation. Previous studies on Aβ aggregation with lipid membranes reported that the surface of lipid membranes served as binding sites for Aβ, which accelerated amyloid aggregation [45,46]. The research with lipid membranes was similar to our case with LK7 aggregates. Besides, the transition time was delayed at each LK7 concentration, indicating that LK7 slowed down the elongation process of fibril growth.

By contrast, cLK7 extended the lag time at all tested concentrations, and showed a concentration-dependent manner, namely the lag time increased with increasing cLK7 concentration (Fig. 2(b), Table 1). The transition times showed a similar concentration dependency. In the presence of 200 μmol/L cLK7, the transition time increased from 8.3 h (pure Aβ_{40}) to 17.1 h. These results suggest that cLK7 inhibited Aβ_{40} fibrillation through extending the lag phase and delaying the elongation phase.

Table 1 Lag time (T_{lag}) and transition time (T_{trans}) for aggregation kinetics of 25 μmol/L Aβ_{40} in the presence of different concentrations of LK7 or cLK7

Concentration /(μmol·L^{-1})	T_{lag} /h	T_{trans} /h
LK7		
0	14.5±1.1	8.3±0.8
25	14.9±0.9	8.9±1.0
50	14.5±0.8	11.5±1.5
100	15.0±0.6	15.2±1.6
200	12.1±1.4	16.2±2.7
cLK7		
0	14.5±1.1	8.3±0.8
25	15.4±2.2	9.3±1.8
50	16.2±1.2	11.0±1.6
100	17.6±0.9	11.9±2.7
200	20.1±1.0	17.1±3.3

An increase in the duration of the lag phase with an inhibitor was generally regarded to the stabilizing effect of the inhibitor by stabilizing the unordered-soluble monomers or small oligomers and delaying the conformational shift [47]. Thus, the results indicate that cLK7 would stabilize the initial conformation of Aβ_{40}, resulting in the elongation of the lag phase. Namely, cLK7 could not only suppress the fibrillation, but also strongly inhibit the nucleation of the amyloid protein.

TEM was used to study the morphology of Aβ_{40} aggregates formed in the absence and presence of LK7 or cLK7. It is clear in Fig. 3(a) that after incubation for 72 h, Aβ_{40} alone aggregated into abundant well-defined fibrils in length of several micrometers. In the presence of 25 μmol/L LK7 (Aβ_{40}/LK7 = 1:1), there was no obvious effect on the morphology of Aβ_{40} fibrils (Fig. 3(b)).

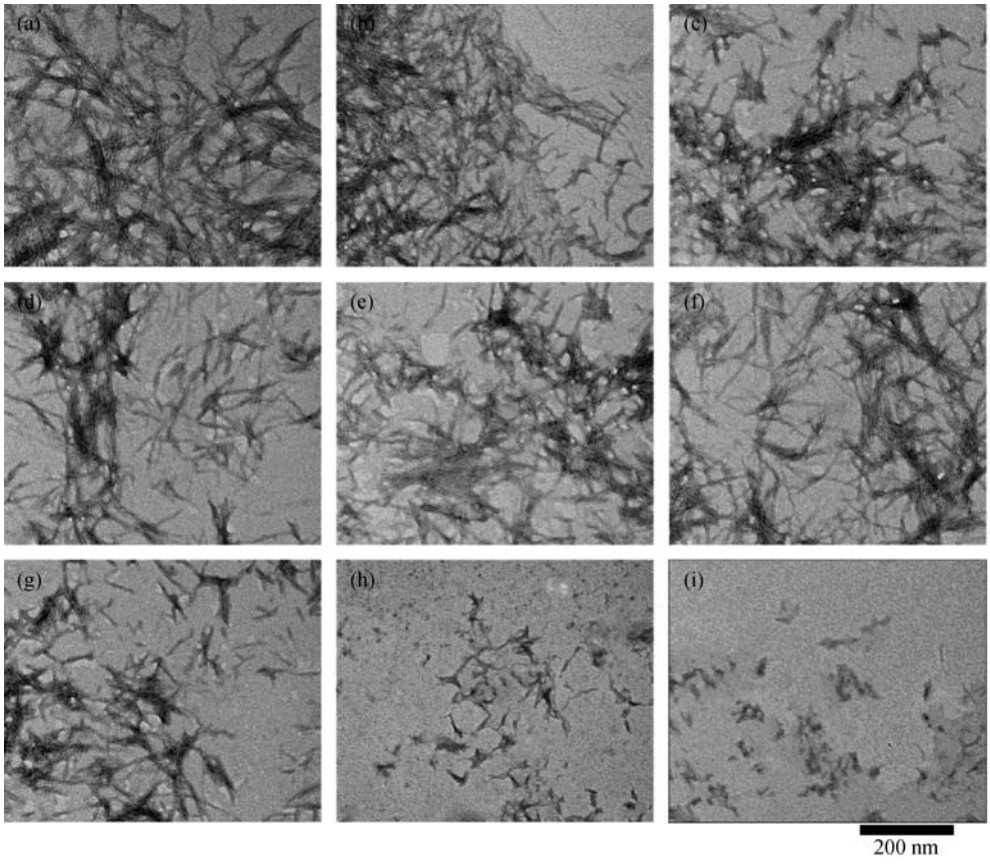

Fig. 3 TEM images of Aβ_{40} (25 μmol/L) in the absence and presence of LK7 and cLK7. (a) Aβ_{40} alone; (b to e) Aβ_{40} with LK7 at concentrations of (b) 25 μmol/L, (c) 50 μmol/L, (d) 100 μmol/L and (e) 200 μmol/L; (f to i) Aβ_{40} with cLK7 at concentrations of (f) 25 μmol/L, (g) 50 μmol/L, (h) 100 μmol/L and (i) 200 μmol/L. The scale bar of 200 nm is for all the images. All samples were taken after incubation at 37 °C for 72 h

Increasing LK7 concentration, Aβ_{40} was observed to remain in fibrillar form, but much shorter and dispersed (Figs. 3(c) and 3(d)). When the ratio of Aβ_{40}/LK7 was as high as 1:8, more fibrils were observed (Fig. 3(e)) than the case of molar ratio 1:4 (Fig. 3(d)). This result was accordant with the enhanced ThT intensities at Aβ_{40}/LK7 = 1:8 (Figs. 2(a) and S3). By contrast, in the incubation of Aβ_{40} with cLK7, the morphology of Aβ_{40} aggregates changed completely. At low concentrations of cLK7 (Aβ_{40}/cLK7 = 1:1 and 1:2), there were still some fibrils, but the amount and density of fibrils decreased dramatically (Figs. 3(f) and 3(g)). At 100 μmol/L cLK7 (Aβ_{40}/cLK7 = 1:4), there were only short and tiny broken fibrils (Fig. 3(h)). When Aβ_{40} was incubated with 8-fold molar excess of cLK7, the fibrous aggregates disappeared completely but amorphous particles formed (Fig. 3(i)). Combined with the ThT fluorescent analysis (Fig. 2(b)), we conclude that cLK7 suppressed the on-pathway Aβ_{40} aggregation and redirected it into an off-pathway mechanism [16,48].

Previous studies have proven that the formation of β-sheet-rich structure is a crucial early step in amyloidogenesis and on-pathway Aβ fibrils have a characteristic cross-β conformation [49]. To examine the effect of LK7 and cLK7 on the conformational transition of Aβ_{40} during its aggregation, CD spectra of Aβ_{40} incubated without and with the two peptides were determined. In the absence of the peptide inhibitors, the freshly prepared Aβ_{40} exhibited a random coil structure with a negative minimum ellipticity around 200 nm, and after incubation for 72 h, a shift of the minimum ellipticity to 217 nm was observed (Figs. 4(a) and 4(b)), indicating the formation of β-sheet-rich conformation [50]. The quantitative analysis results listed in Table S2 clearly presented this transition. The main secondary structures of the fresh pure Aβ_{40} were helix (18.6%), antiparallel β-sheet (25.5%) and unordered structures (46.2%). After incubation for 72 h, the secondary structural contents changed into 5.2% helix, 22.2% antiparallel β-sheet, 39.4% parallel β-sheet, 8.4% turn, and 24.8% others. Many other studies on Aβ_{40} fibril also reported that the in-register parallel β-sheet was the main content of its secondary structure [51,52].

Considering that both LK7 and cLK7 showed a positive signal at 215–217 nm in their CD spectra (Figs. S1(a) and

S1(b)), which might obscure the signal at 217 nm arising from the Aβ_{40}, spectra of the peptide inhibitors alone were subtracted from spectra of the co-incubations of the peptides and Aβ_{40}, as done in literature [53], to leave normalized CD spectra accounting for the effect of peptides upon Aβ_{40}. As shown in Fig. 4(a), Aβ_{40} (25 μmol/L) incubation with LK7 of low concentrations ($\leqslant$100 μmol/L) gave an upward shift of ellipticity above 217 nm, reflecting a reduction of β-sheet content. In detail, both antiparallel and parallel β-sheet content decreased (expect for the antiparallel β-sheet in the Aβ_{40}:LK7 = 1:1, which was similar), and the decreases in the antiparallel β-sheet content were more prominent, both of which led to the increase of unordered structures (others) (Table S2). However, when Aβ_{40} was incubated with LK7 in a molar ratio of Aβ_{40}:LK7 = 1:8, a large amount of β-sheet structure emerged, and the total β-sheet (antiparallel + parallel) was 55.7%, almost equal to the Aβ_{40} only system (61.6%) after cultured for 72 h. The results might be attributed to the self-assembly of LK7 (Fig. 1(a)). This weaker inhibition of β-sheet formation by LK7 supported the results of ThT and TEM assays, suggesting that high LK7 concentration was detrimental.

For the co-incubation of Aβ_{40} with cLK7, the ellipticity above 217 nm also showed an upward shift by increasing the molar ratio of Aβ_{40}/cLK7 from 1:1 to 1:4 (Fig. 4(b)). The total β-sheet contents in the presence of cLK7 decreased in a concentration-dependent manner (Table S2), showing the effectiveness of cLK7 on the inhibition of Aβ_{40} conformational transition to β-sheet. It is notable that those β-sheet structures of Aβ_{40}-cLK7 co-incubation samples were stacked in an antiparallel way, while those of pure Aβ_{40} fibrils were arranged in parallel at 72 h (Table S2), proving cLK7 changed the pathway of conformational transition of Aβ_{40} aggregation. Moreover, in a molar ratio of 1:8, the helix (20.4%) and the others (38.5%) were comparable to those of Aβ_{40} alone at the beginning (18.6% helix and 46.2% others at 0 h), indicating that cLK7 could stabilize the initial secondary structures of Aβ_{40}. The CD results could also help understand the results in Fig. 2(b) and Table 1, as cLK7 could elongate the lag phase by its stabilizing effect. A similar phenomenon was observed by Liu et al. [54], who thought that the binding affinity of their inhibitor (RYYAAFFARR) for Aβ_{40} was strong enough to stabilize the initial secondary structure of Aβ_{40}. Hence, we infer that the head-to-tail cyclization would enhance the binding affinity of cLK7 for Aβ_{40}, make cLK7 efficiently bind Aβ_{40} monomers, and thus stabilize the initial secondary structures of Aβ_{40}, which suppressed Aβ_{40} aggregation into the on-pathway parallel β-sheet structures and induced Aβ_{40} to form the off-pathway aggregates, as shown by the TEM images (Figs. 3(h) and 3(i)).

3.3 Effects of LK7 and cLK7 on Aβ_{40} cytotoxicity

Aβ_{40} aggregates are known to exert obvious cytotoxicity on neuronal cells, and the toxicity depends on the species of aggregates (soluble oligomers, protofibrils and fibrils) [5,54]. MTT assays were performed to assess the effects of LK7 and cLK7 on the cytotoxicity of Aβ_{40} aggregates on SH-SY5Y cells (Fig. 5). The cell viability after Aβ_{40} treatment was left at about 66% of the control. By incubation of Aβ_{40} with LK7, the cell viability moderately increased at low concentrations (Aβ_{40}:LK7 = 1:1 and 1:2). However, further increase of LK7 concentration caused a continuous decline in the cell viability. The cell viability in Aβ_{40}:LK7 = 1:8 was only 61%, even lower than that in the Aβ_{40} only system (66%), suggesting the invalidation of LK7 of high concentration on reducing the cytotoxicity of Aβ_{40}. This is probably because at high LK7 concentrations, the toxicity of LK7 aggregates is greater than its detoxification effect, as can be seen from Fig. 1(d).

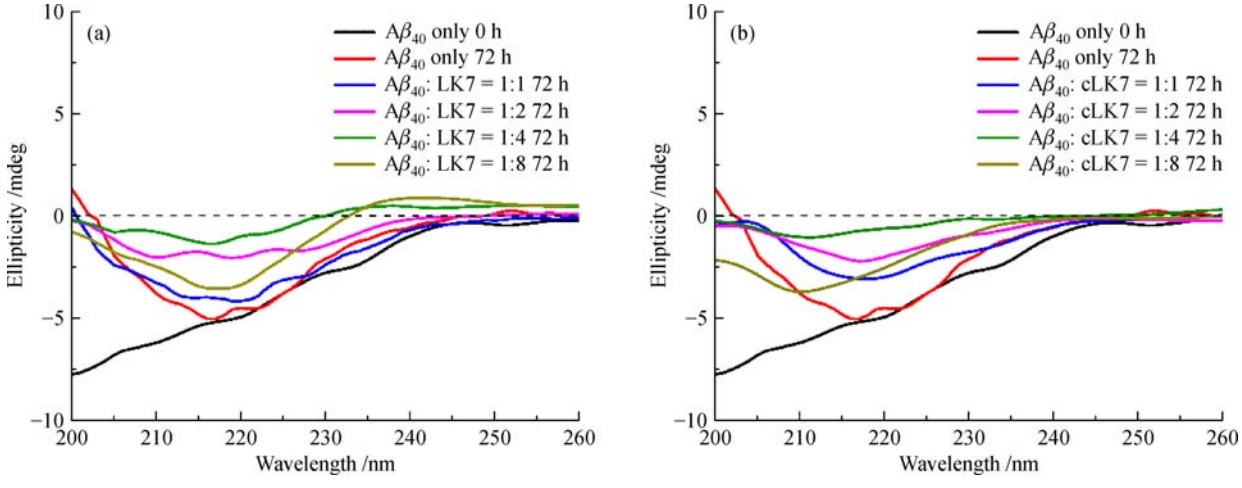

Fig. 4 Far-UV circular dichroism spectra of Aβ_{40} (25 μmol/L) incubated in the absence and presence of different concentrations of (a) LK7 and (b) cLK7. The co-incubation of Aβ_{40} was conducted at 37 °C

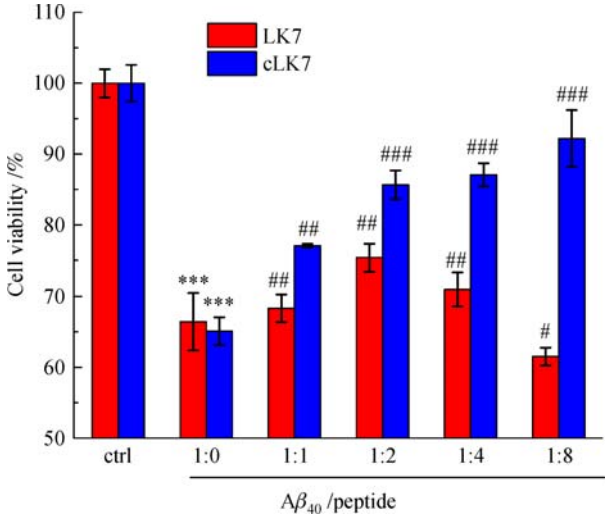

Fig. 5 Inhibitory effects of LK7 and cLK7 on Aβ_{40}-induced cytotoxicity for SH-SY5Y cell lines: ***$p < 0.001$, compared to control groups; #$p < 0.05$, ##$p < 0.01$, ###$p < 0.001$, compared to the Aβ_{40} treated group (Aβ_{40} only)

By contrast, the cell viability increased with increasing the concentration of cLK7, up to 92% at Aβ_{40}:cLK7 = 1:8. Thus, the superiority of cLK7 over LK7 was demonstrated by the MTT assays.

3.4 Analyses of molecular interactions

The above ThT fluorescence, TEM observation, CD spectroscopy and cell viability analysis have demonstrated that cLK7 was superior over LK7 in inhibiting Aβ_{40} fibrillation and cytotoxicity. To reveal the mechanisms of the superior effects of cLK7 over LK7, we scrutinized the nature of the molecular interactions between Aβ_{40} and the two peptides by ITC.

ITC measurement can reveal the thermodynamic interactions between Aβ_{40} and its inhibitor. Thermodynamic parameters obtained from the ITC experiments (Figs. S4(a) and S4(b)) are listed in Table 2. The Wiseman's *C*-parameter values for evaluating the fittings were 1.11 and 5.39 for LK7 and cLK7, respectively, proving the reliability of our results [36,37]. The negative ΔH values and positive ΔS values revealed the contributions of electrostatic interactions and hydrogen boding as well as hydrophobic interactions based on the Ross and Subramanian's description on thermodynamic parameter

Table 2 Thermodynamic parameters for the interactions between the inhibitors and Aβ_{40} at 37 °C

	LK7	cLK7
K_D/(μmol·L^{-1})	32.2±1.5	4.96±0.25
ΔH/(kcal·mol^{-1})	−4.25±0.18	−4.92±0.27
$T\Delta S$/(kcal·mol^{-1})	2.12±0.06	2.61±0.14
ΔG/(kcal·mol^{-1})	−6.37±0.24	−7.53±0.41

associated with various individual kinds of interactions that may take place in protein association processes [55]. The electrostatic interactions and hydrogen bonding were the main driving forces for the interactions of Aβ_{40} with both LK7 and cLK7, because the absolute values of ΔH (negative) for both the peptides were about two times larger than those of $T\Delta S$ (positive). It is noteworthy that both the ΔH and ΔS values for cLK7 were higher than those for LK7 (Table 2). This suggests that the cyclization may enhance the molecular interactions of the peptide (cLK7) with Aβ_{40}, making it present a binding affinity over six times higher than LK7 as seen from the dissociation constant (K_D). This is in agreement with the report by Ziehm et al. [24] that the cyclization enhanced the binding affinity of peptides for Aβ about two times. Cairo et al. [56] suggested that ligands exhibiting higher affinity for Aβ were more effective in altering its aggregation and inhibiting its cytotoxicity. Furthermore, the binding affinity for cLK7 and Aβ_{40} (K_D = 4.96 μmol/L) is superior or comparable to most of the recently reported peptide inhibitors, such as cD3 (K_D = 6.7 μmol/L) [24], LPFFD (K_D = 156 μmol/L) and RR (K_D = 1.1 μmol/L) [54]. As for LK7, its binding affinity (K_D = 32.2 μmol/L) is lower than cLK7, thereafter its inhibitory effect is also poor. So, the significantly increased binding affinity of cLK7 for Aβ_{40} could well explain its enhanced inhibition effects on the amyloid fibrillation and cytotoxicity.

Based on the above experimental results, a mechanistic model is proposed. For the on-pathway fibrillogenesis of Aβ_{40} (Fig. 6(a)), Aβ monomers first undergo a transition from random coil into β-sheet-rich structures, most of which are parallel arrangement, and then assemble into amyloid fibrils via several metastable oligomers and protofibrils of cross-β conformations, both of which are highly toxic [57]. This amyloid formation at least includes two microscopic steps: Primary nucleation, in which monomers in solution form nuclei, and fibril elongation, in which monomers add to the ends of existing aggregates and lead to their growth [43]. Any interference to the two steps would have a significant impact on the overall aggregation kinetics.

In the presence of LK7 (Fig. 6(b)), there existed an optimal concentration to achieve moderate inhibition of Aβ_{40} fibrillation. At low concentrations ($\leqslant$100 μmol/L, below the optimal concentration), LK7 could interact with Aβ_{40} and interfere the conformational changes of Aβ_{40} from random coil to β-sheet rich structures (Fig. 4(a), Table S2), but parallel arrangement as the major β-sheet structures of Aβ_{40} could not be affected (Table S2). So LK7 could not change the lag time for nucleation but extend the elongation time of Aβ_{40} fibrillation moderately (Fig. 2(a), Table 1), leading to the decrease in density and length of fibrils (Figs. 3(b–d)). Furthermore, less protofibrils and fibrils would gave slightly lower cytotoxicity and higher cell viability. With the increase of LK7 concentration above the optimal concentration, LK7

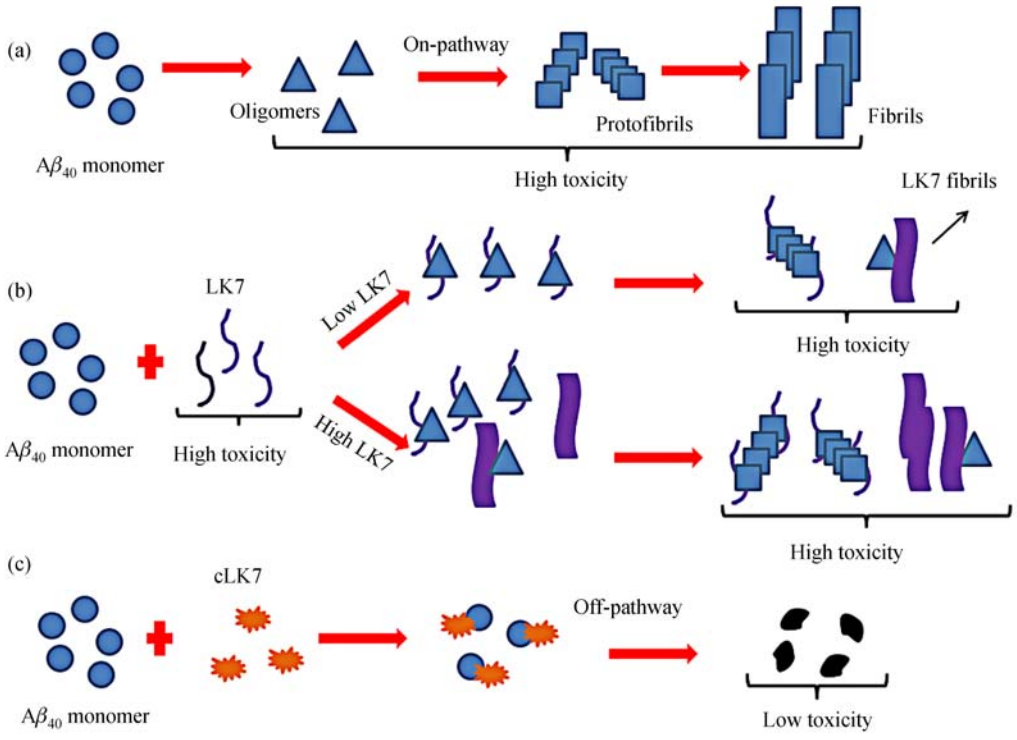

Fig. 6 Schematic representations of Aβ_{40} aggregation and cytotoxicity: (a) on-pathway aggregation of Aβ_{40} monomers, (b) Aβ_{40} aggregation in the presence of LK7, and (c) Aβ_{40} aggregation in the presence of cLK7

would prefer to self-assemble into fibrils (Fig. 1(a)) rather than interact with Aβ_{40} because of its low affinity for Aβ_{40} (Table 2), so less free LK7 molecules were left for interacting with Aβ_{40}, leading to decreased inhibition effects, as confirmed by the increased ThT fluorescence intensity (Figs. 2(a) and S3), more emerged fibrils (Fig. 3(e)) and higher β-sheet contents (Fig. 4(a), Table S2). Similar phenomenon was observed in literature [20], in which the cyclic peptide CG3, designed by mimicking the Aβ binding domain on transthyretin, showed a decrease in the efficacy at inhibiting Aβ fibrillogenesis with increasing CG3 concentration owing to its self-assembly characteristic. Moreover, the toxicity of LK7 fibrils at higher concentrations (Fig. 1(d)) would add to amyloid toxicity as evidenced by the cell viability assays (Fig. 5). The toxicity of LK7 itself could also explain why the optimal concentration for inhibiting Aβ_{40} fibrillation (Aβ_{40}:LK7 = 1:4, Figs. 2(a) and S3) was different from its optimal detoxification concentration (Aβ_{40}:LK7 = 1:2, Fig. 5).

By contrast, cLK7 inhibited Aβ_{40} fibrillation and cytotoxicity in a dose-dependent manner. The binding affinity of cLK7 for Aβ_{40} was strikingly enhanced (K_D = 4.96 μmol/L) (Table 2). Moreover, cLK7 had very weak tendency to aggregate and formed small spherical particles (Fig. 1(b)) that were little toxic (Fig. 1(d)). Thus, cLK7 could efficiently bind to Aβ_{40} monomers instead of self-aggregation (Fig. 6(c)). The strong binding could not only inhibit the fibrillation, but also inhibit the nucleation in the early stage of the amyloid self-assembling (Fig. 2(b)) by stabilizing non-amyloidogenic conformation and suppressing the on-pathway formation of parallel β-sheet structure (Fig. 4(b), Table S2). So off-pathway aggregates formed (Fig. 3(i)), which had no or less toxicity (Fig. 5). Thus, cLK7 offered an inhibitory effect on the amyloid aggregation and cytotoxicity at a wide concentration range.

4 Conclusions

We have synthesized a cyclic peptide cLK7 by the head-to-tail cyclization of a previously designed peptide inhibitor, LVFFARK, for amyloid β-proteins and extensively characterized the two counterparts. The cyclization not only significantly increases the peptide stability against proteolysis but also changes its self-assembling behavior. LK7 is prone to self-assembling into long and dense fibrils that are highly cytotoxic, whereas cLK7 aggregates into less and small spherical particles of little cytotoxicity. Moreover, the cyclization distinctly increases the interactions between cLK7 with Aβ_{40}, leading to a six-time increase of the binding affinity for Aβ_{40} by electrostatic interaction, hydrogen bonding and hydrophobic interaction. The strong binding of cLK7 stabilizes the initial secondary structure of Aβ_{40}, induces the formation of off-

pathway amorphous aggregates, and makes the cyclic peptide a potent inhibitor on the nucleation and elongation of Aβ_{40} fibrils. Thus, cLK7 significantly suppresses the amyloid cytotoxicity. By comparison, LK7 could not stabilize the secondary structure of Aβ_{40} and inhibit the nucleation of the amyloid protein, and it could only provide moderate inhibition effect at lower concentrations. Moreover, its strong tendency of self-assembly into fibrils could compromise its inhibition effect, so it shows little inhibitory capability at higher concentrations. The results suggest that the peptide cyclization is a promising strategy in the design and development of novel peptide inhibitors against Aβ aggregation.

Acknowledgements This work was supported by the National Natural Science Foundation of China (Grant Nos. 21376172, 21406160, 21528601 and 21621004) and the Natural Science Foundation of Tianjin from Tianjin Municipal Science and Technology Commission (Contract No. 16JCZDJC32300).

Electronic Supplementary Material Supplementary material is available in the online version of this article at https://doi.org/10.1007/s11705-017-1687-2 and is accessible for authorized users.

References

1. Goedert M, Spillantini M G. A century of Alzheimer's disease. Science, 2006, 314(5800): 777–781
2. Hardy J, Selkoe D J. The amyloid hypothesis of Alzheimer's disease: Progress and problems on the road to therapeutics. Science, 2002, 297(5580): 353–356
3. Knowles T P, Vendruscolo M, Dobson C M. The amyloid state and its association with protein misfolding diseases. Nature Reviews. Molecular Cell Biology, 2014, 15(6): 384–396
4. Selkoe D J. Soluble oligomers of the amyloid β-protein impair synaptic plasticity and behavior. Behavioural Brain Research, 2008, 192(1): 106–113
5. Chimon S, Shaibat M A, Jones C R, Calero D C, Aizezi B, Ishii Y. Evidence of fibril-like β-sheet structures in a neurotoxic amyloid intermediate of Alzheimer's β-amyloid. Nature Structural & Molecular Biology, 2008, 14(12): 1157–1164
6. Härd T, Lendel C. Inhibition of amyloid formation. Journal of Molecular Biology, 2012, 421(4): 441–465
7. Wang Q M, Yu X, Li L Y, Zheng J. Inhibition of amyloid-β aggregation in Alzheimer's disease. Current Pharmaceutical Design, 2014, 20(8): 1223–1243
8. Craik D J, Fairlie D P, Liras S, Price D. The future of peptide-based drugs. Chemical Biology & Drug Design, 2013, 81(1): 136–147
9. Tjernberg L O, Näslund J, Lindqvist F, Johansson J, Karlström A R, Thyberg J, Terenius L, Nordstedt C. Arrest of β-amyloid fibril formation by a pentapeptide ligand. Journal of Biological Chemistry, 1996, 271(15): 8545–8548
10. Liu F F, Du W J, Sun Y, Zheng J, Dong X Y. Atomistic characterization of binding modes and affinity of peptide inhibitors to amyloid-β protein. Frontiers of Chemical Science and Engineering, 2014, 8(4): 433–444
11. Soto C, Kindy M S, Baumann M, Frangione B. Inhibition of Alzheimer's amyloidosis by peptides that prevent β-sheet conformation. Biochemical and Biophysical Research Communications, 1996, 226(3): 672–680
12. Bansal S, Maurya I K, Yadav N, Thota C K, Kumar V, Tikoo K, Chauhan V S, Jain R. *C*-terminal fragment, A$\beta_{32\text{-}37}$, analogues protect against Aβ aggregation-induced toxicity. ACS Chemical Neuroscience, 2016, 7(5): 615–623
13. Fradinger E A, Monien B H, Urbanc B, Lomakin A, Tan M, Li H, Spring S M, Condron M M, Cruz L, Xie C W, Benedek G B, Bitan G. *C*-terminal peptides coassemble into Aβ_{42} oligomers and protect neurons against Aβ_{42}-induced neurotoxicity. Proceedings of the National Academy of Sciences of the United States of America, 2008, 105(37): 14175–14180
14. Takahashi T, Mihara H. Peptide and protein mimetics inhibiting amyloid β-peptide aggregation. Accounts of Chemical Research, 2008, 41(10): 1309–1318
15. Turner J P, Lutzrechtin T, Moore K A, Rogers L, Bhave O, Moss M A, Servoss S L. Rationally designed peptoids modulate aggregation of amyloid-β_{40}. ACS Chemical Neuroscience, 2014, 5(7): 552–558
16. Arai T, Sasaki D, Araya T, Sato T, Sohma Y, Kanai M. A cyclic KLVFF-derived peptide aggregation inhibitor induces the formation of less-toxic off-pathway amyloid-β oligomers. ChemBioChem, 2014, 15(17): 2577–2583
17. Xiong N, Dong X Y, Zheng J, Liu F F, Sun Y. Design of LVFFARK and LVFFARK-functionalized nanoparticles for inhibiting amyloid β-protein fibrillation and cytotoxicity. ACS Applied Materials & Interfaces, 2015, 7(10): 5650–5662
18. Arai T, Araya T, Sasaki D, Taniguchi A, Sato T, Sohma Y, Kanai M. Rational design and identification of a non-peptidic aggregation inhibitor of amyloid-β based on a pharmacophore motif obtained from cyclo [-Lys-Leu-Val-Phe-Phe-]. Angewandte Chemie International Edition, 2014, 53(31): 8236–8239
19. Luo J H, Otero J M, Yu C H, Wärmländer S K, Gräslund A, Overhand M, Abrahams J P. Inhibiting and reversing amyloid-β peptide (1–40) fibril formation with gramicidin S and engineered analogues. Chemistry (Weinheim an der Bergstrasse, Germany), 2013, 19(51): 17338–17348
20. Cho P Y, Joshi G, Boersma M D, Johnson J A, Murphy R M. A cyclic peptide mimic of the β-amyloid binding domain on transthyretin. ACS Chemical Neuroscience, 2015, 6(5): 778–789
21. Zheng J, Baghkhanian A M, Nowick J S. A hydrophobic surface is essential to inhibit the aggregation of a Tau-protein-derived hexapeptide. Journal of the American Chemical Society, 2013, 135(18): 6846–6852
22. Richman M, Wilk S, Chemerovski M, Wärmländer S K T S, Wahlström A, Gräslund A, Rahimipour S. *In vitro* and mechanistic studies of an antiamyloidogenic self-assembled cyclic D,L-α-peptide architecture. Journal of the American Chemical Society, 2013, 135 (9): 3474–3484
23. Choi S J, Jeong W J, Kang S K, Lee M, Kim E, Ryu D Y, Lim Y B. Differential self-assembly behaviors of cyclic and linear peptides. Biomacromolecules, 2012, 13(7): 1991–1995
24. Ziehm T, Brener O, Groen T, Kadish I, Frenzel D, Tusche M, Kutzsche J, Reiss K, Gremer L, Nagel-Steger L, et al. Increase of positive net charge and conformational rigidity enhances the

efficacy of D-enantiomeric peptides designed to eliminate cytotoxic Aβ species. ACS Chemical Neuroscience, 2016, 7(8): 1088–1096

25. March D R, Abbenante G, Bergman D A, Brinkworth R I, Wickramasinghe W, Begun J, Martin J L, Fairlie D P. Substrate-based cyclic peptidomimetics of Phe-Ile-Val that Inhibit HIV-1 protease using a novel enzyme-binding mode. Journal of the American Chemical Society, 1996, 118(14): 3375–3379
26. Rezai T, Yu B, Millhauser G L, Jacobson M P, Lokey R S. Testing the conformational hypothesis of passive membrane permeability using synthetic cyclic peptide diastereomers. Journal of the American Chemical Society, 2006, 128(8): 2510–2511
27. Wang Q M, Shah N, Zhao J, Wang C, Zhao C, Liu L, Li L Y, Zhou F, Zheng J. Structural, morphological, and kinetic studies of β-amyloid peptide aggregation on self-assembled monolayers. Physical Chemistry Chemical Physics, 2011, 13(33): 15200–15210
28. Gordon D J, Sciarretta K L, Meredith S C. Inhibition of β-amyloid (40) fibrillogenesis and disassembly of β-amyloid (40) fibrils by short β-amyloid congeners containing *N*-methyl amino acids at alternate residues. Biochemistry, 2001, 40(28): 8237–8245
29. Ferrie J J, Gruskos J J, Goldwaser A L, Decker M E, Guarracino D A. A comparative protease stability study of synthetic macrocyclic peptides that mimic two endocrine hormones. Bioorganic & Medicinal Chemistry Letters, 2013, 23(4): 989–995
30. Yu R, Seymour V A L, Berecki G, Jia X, Akcan M, Adams D J, Kaas Q, Craik D J. Less is more: Design of a highly stable disulfide-deleted mutant of analgesic cyclic α-conotoxin Vc1.1. Scientific Reports, 2015, 5(1): 13264
31. Cheng P N, Liu C, Zhao M, Eisenberg D, Nowick J S. Amyloid β-sheet mimics that antagonize protein aggregation and reduce amyloid toxicity. Nature Chemistry, 2012, 4(11): 927–933
32. Cabaleiro-Lago C, Szczepankiewicz O, Linse S. The effect of nanoparticles on amyloid aggregation depends on the protein stability and intrinsic aggregation rate. Langmuir, 2012, 28(3): 1852–1857
33. Luo J H, Yu C H, Yu H X, Borstnar R, Kamerlin S C, Gräslund A, Abrahams J P, Wärmländer S K. Cellular polyamines promote amyloid-beta (Aβ) peptide fibrillation and modulate the aggregation pathways. ACS Chemical Neuroscience, 2013, 4(3): 454–462
34. Micsonai A, Wien F, Kernya L, Lee Y H, Goto Y, Réfrégiers M, Kardos J. Accurate secondary structure prediction and fold recognition for circular dichroism spectroscopy. Proceedings of the National Academy of Sciences of the United States of America, 2015, 112(24): 3095–3103
35. Choi H J, Huber A H, Weis W I. Thermodynamics of β-catenin-ligand interactions: The roles of the *N*- and *C*-terminal tails in modulating binding affinity. Journal of Biological Chemistry, 2006, 281(2): 1027–1038
36. Wiseman T, Williston S, Brandts J F, Lin L N. Rapid measurement of binding constants and heats of binding using a new titration calorimeter. Analytical Biochemistry, 1989, 179(1): 131–137
37. Freyer M W, Lewis E A. Isothermal titration calorimetry: Experimental design, data analysis, and probing macromolecule/ligand binding and kinetic interactions. Methods in Cell Biology, 2008, 84: 79–113
38. Fotakis G, Timbrell J A. *In vitro* cytotoxicity assays: Comparison of LDH, neutral red, MTT and protein assay in hepatoma cell lines following exposure to cadmium chloride. Toxicology Letters, 2006, 160(2): 171–177
39. Gupta M, Bagaria A, Mishra A, Mathur P, Basu A, Ramakumar S, Chauhan V S. Self-assembly of a dipeptide-containing conformationally restricted dehydrophenylalanine residue to form ordered nanotubes. Advanced Materials, 2007, 19(6): 858–861
40. Huang R L, Su R X, Qi W, Zhao J, He Z M. Hierarchical, interface-induced self-assembly of diphenylalanine: Formation of peptide nanofibers and microvesicles. Nanotechnology, 2011, 22(24): 245609
41. Biancalana M, Koide S. Molecular mechanism of thioflavin-T binding to amyloid fibrils. Biochimica et Biophysica Acta (BBA)-Proteins Proteomics, 2010, 1804(7): 1405–1412
42. Cohen S I, Linse S, Luheshi L M, Hellstrand E, White D A, Rajah L, Otzen D E, Vendruscolo M, Dobson C M, Knowles T P. Proliferation of amyloid-β_{42} aggregates occurs through a secondary nucleation mechanism. Proceedings of the National Academy of Sciences of the United States of America, 2013, 110(24): 9758–9763
43. Arosio P, Knowles T P, Linse S. On the lag phase in amyloid fibril formation. Physical Chemistry Chemical Physics, 2015, 17(12): 7606–7618
44. Zhao Z J, Zhu L, Li H Y, Cheng P, Peng J X, Yin Y D, Yang Y, Wang C, Hu Z Y, Yang Y L. Antiamyloidogenic activity of Aβ_{42}-binding peptoid in modulating amyloid oligomerization. Small, 2017, 13(1): 1602857
45. Sugiura Y, Ikeda K, Nakano M. High membrane curvature enhances binding, conformational changes, and fibrillation of amyloid-β on lipid bilayer surfaces. Langmuir, 2015, 31(42): 11549–11557
46. Nagarathinam A, Höflinger P, Bühler A, Schäfer C, Mcgovern G, Jeffrey M, Staufenbiel M, Jucker M, Baumann F. Membrane-anchored Aβ accelerates amyloid formation and exacerbates amyloid-associated toxicity in mice. Journal of Neuroscience, 2013, 33(49): 19284–19294
47. Bartolini M, Bertucci C, Bolognesi M L, Cavalli A, Melchiorre C, Andrisano V. Insight into the kinetic of amyloid-β (1–42) peptide self-aggregation: Elucidation of inhibitors' mechanism of action. ChemBioChem, 2007, 8(17): 2152–2161
48. Ehrnhoefer D E, Bieschke J, Boeddrich A, Herbst M, Masino L, Lurz R, Engemann S, Pastore A, Wanker E E. EGCG redirects amyloidogenic polypeptides into unstructured, off-pathway oligomers. Nature Structural & Molecular Biology, 2008, 15(6): 558–566
49. Du W J, Guo J J, Gao M T, Hu S Q, Dong X Y, Han Y F, Liu F F, Jiang S, Sun Y. Brazilin inhibits amyloid β-protein fibrillogenesis, remodels amyloid fibrils and reduces amyloid cytotoxicity. Scientific Reports, 2015, 5(1): 7992
50. Kumar S, Udgaonkar J B. Mechanisms of amyloid fibril formation by proteins. Current Science, 2010, 98(5): 639–656
51. Tu Y L, Ma S, Liu F F, Sun Y, Dong X Y. Hematoxylin inhibits amyloid β-protein fibrillation and alleviates amyloid-induced cytotoxicity. Journal of Physical Chemistry B, 2016, 120(44): 11360–11368
52. Qiang W, Yau W M, Luo Y, Mattson M P, Tycko R. Antiparallel β-sheet architecture in iowa-mutant β-amyloid fibrils. Proceedings of the National Academy of Sciences of the United States of America, 2012, 109(12): 4443–4448

53. Acerra N, Kad N M, Griffith D A, Ott S, Crowther D C, Mason J M. Retro-inversal of intracellular selected β-amyloid-interacting peptides: Implications for a novel Alzheimer's disease treatment. Biochemistry, 2014, 53(13): 2101–2111
54. Liu J, Wang W, Zhang Q, Zhang S H, Yuan Z. Study on the efficiency and interaction mechanism of a decapeptide inhibitor of β-amyloid aggregation. Biomacromolecules, 2014, 15(3): 931–939
55. Ross P D, Subramanian S. Thermodynamics of protein association reactions: Forces contributing to stability. Biochemistry, 1981, 20 (11): 3096–3102
56. Cairo C W, Strzelec A, Murphy R M, Kiessling L L. Affinity-based inhibition of β-amyloid toxicity. Biochemistry, 2002, 41(27): 8620–8629
57. Liao Y H, Chang Y J, Yoshiike Y, Chang Y C, Chen Y R. Negatively charged gold nanoparticles inhibit Alzheimer's amyloid-β fibrillization, induce fibril dissociation, and mitigate neurotoxicity. Small, 2012, 8(23): 3631–3639